Journal of Asian Earth Sciences 58 (2012) 143–157

Contents lists available at SciVerse ScienceDirect

Journal of Asian Earth Sciences

journal homepage: www.elsevier.com/locate/jseaes

The origin of Eo- and Neo-himalayan granitoids, Eastern Tibet

Amos B. Aikman [a], T. Mark Harrison [b,*], Joerg Hermann [a]

[a] Research School of Earth Sciences, Australian National University, Canberra, ACT 0200, Australia
[b] Department of Earth and Space Sciences, University of California, Los Angeles, CA 90095, USA

ARTICLE INFO

Article history:
Received 13 September 2011
Received in revised form 20 April 2012
Accepted 21 May 2012
Available online 9 June 2012

Keywords:
Himalaya
Magmatism
Zircon
Water-saturated melting

ABSTRACT

Two distinctive modes of post-collisional magmatism are evident along a transect through the eastern Himalaya at ca. 92°E. The first comprises Eocene igneous complexes emplaced into the central Tethyan Himalaya Series (THS) (Dala granitoids, 44.1 ± 1.2 Ma) and the core of the Yala-Xiangbo dome (Yala-Xiangbo granitoids, 42 ± 5 Ma). Trace element characteristics and Rb–Sr and Sm–Nd isotopes indicate that the Dala granitoids formed from sub-equal mixtures of Gangdese-type magmas and rocks of the Greater Himalayan Crystallines and/or THS. The Yala-Xiangbo granitoids are geochemically complex but interpreted to be evolved equivalents of the Dala granitoid suite. The undeformed Dala plutons constrain the timing of deformation of THS metasediments to be >44 Ma and their compositions indicates that components of the Indian foreland sequences had been accreted to the hanging wall of the main Himalayan decollement by that time. The second magmatic mode comprises Miocene intrusions (Arunachal- and Tsona-types) similar in most respects to the High Himalayan Leucogranites documented throughout the range. Although fluid-absent melting of metapelites appears to be the dominant origin of Miocene Himalaya leucogranites, thermometry and trace element data for the Arunachal-type intrusions suggest that they formed under fluid-present conditions. Sr and Nd-isotopes indicate that Lesser Himalayan metasediments were involved during the partial melting that produced the Arunachal-type leucogranites.

1. Introduction

The Himalayan orogen is broadly characterized by two belts of Miocene granitoids oriented sub-parallel to the trace of the main Himalayan arc: the High Himalayan Leucogranites (HHLs) and the North Himalayan Granites (NHG) (e.g. LeFort, 1996) (Fig. 1). Studies of Himalayan magmatism have generally focused on Miocene HHL in the central Himalayan arc (e.g. LeFort et al., 1987; England et al., 1992; Harris and Massey, 1994; Davidson et al., 1997; Harrison et al., 1997, 1998a,b). The NHG show a wider range of dominantly Miocene ages (Chen et al., 1990; Harrison et al., 1997; Lee et al., 2000, 2004; Zhang et al., 2004a,b; Quigley et al., 2006, 2008; King et al., 2011) but include rare, Eocene granitoid plutons (Ding et al., 2005; Aikman et al., 2008; Aikman and Harrison, 2011; Pullen et al., 2011; Zeng et al., 2011).

At least five suites of Tertiary granitoids crop out along a N–S transect through the eastern Himalaya and southern Tibet at ca. 92°E (Fig. 2). From north to south, the Gangdese Batholith (GB) is an Andean Cretaceous-Tertiary volcanoplutonic complex north of the Indus-Tsangpo Suture (ITS) (Debon et al., 1986; Harrison et al., 2000); the Yala-Xiangbo granitoids and associated pelites are part of a 42 ± 5 Ma igneous-metamorphic complex (Aikman and Harrison, 2011); the Dala granitoids are undeformed 44.1 ± 1.2 Ma plutons emplaced into deformed sub-greenschist facies metasediments of the Tethyan Himalaya (Aikman et al., 2008; Zeng et al., 2011), ~50 km south of the Yala complex; the Tsona leucogranites are sill- and dyke-like bodies adjacent to the normal-slip South Tibetan Detachment (STD); and the Arunachal leucogranites are sill-like bodies emplaced into the Arunachal crystallines, between the Main Central Thrust (MCT) and STD (Aikman, 2007).

The emplacement style and structural position of the Tsona leucogranites and Arunachal leucogranites is similar to most HHL (see review in Yin and Harrison, 2000). The Yala-Xiangbo granitoids are structurally more similar to the North Himalayan Granites (NHGs) (Aikman et al., 2012, Fig. 1), although they contain notably older ages than typical for the NHG (Chen et al., 1990; Lee et al., 2000, 2004; Zhang et al., 2004a,b; Quigley et al., 2006, 2008; King et al., 2011) that are not well-explained by Himalayan tectonomagmatic models (e.g., LeFort et al., 1987; Pinet and Jaupart, 1987; England et al., 1992; Inger and Harris, 1993; Harris and Massey, 1994; Davidson et al., 1997; Harrison et al., 1997, 1998a,b; Beaumont et al., 2001, 2004).

The distribution and timing of Himalayan granitic magmatism reflects the thermal budget and locus of tectonic activity within

* Corresponding author.
E-mail address: tmark.harrison@gmail.com (T.M. Harrison).

1367-9120/$ - see front matter © 2012 Elsevier Ltd. All rights reserved.
http://dx.doi.org/10.1016/j.jseaes.2012.05.018

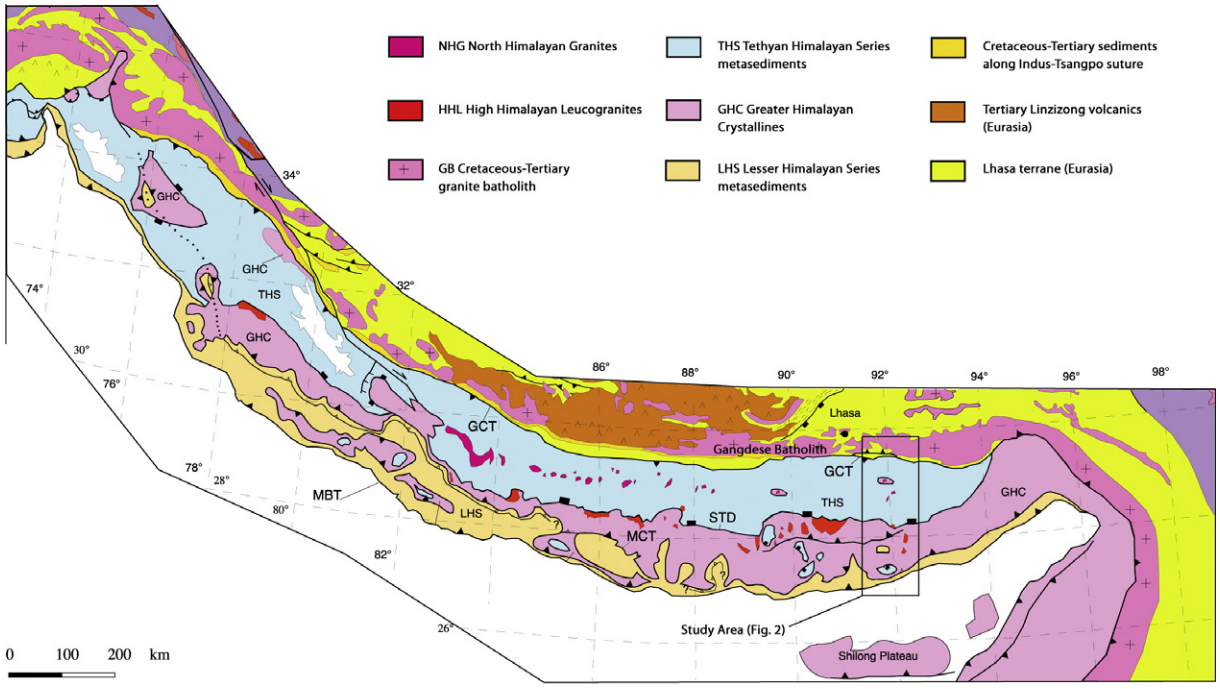

Fig. 1. Regional geological map of the Himalaya (after Yin, 2006). MBT – Main Boundary Thrust; MCT – Main Central Thrust; STD – South Tibetan Detachment; GCT – Great Counter Thrust; red box shows location of Fig. 2. (For interpretation of the references to color in this figure legend, the reader is referred to the web version of this article.)

the orogen (e.g. LeFort et al., 1987; Yin and Harrison, 2000), while knowledge of granitoid geochemistry can help identify the distribution of protolith materials (e.g., Deniel et al., 1987; Inger and Harris, 1993). Thus in this paper we document major and trace element and Sr–Nd isotopic data on a well-dated (Aikman and Harrison, 2011) sample suite collected along a N–S traverse at ca. 92°E. Our results suggest magmatism is due to a broader range of processes than typically thought for the Himalaya and challenge existing evolutionary models (e.g., LeFort, 1975; Harrison et al., 1998a,b; Beaumont et al., 2004).

2. Analytical methods

2.1. Sample selection

This study utilized the samples documented in Aikman and Harrison (2011) as well as 15 mafic rock samples from exposures along the ITS and throughout the Tethyan Himalaya, chosen to test for a genetic relationship with Himalayan granitoids. Table 1 summarizes the U–Pb ages of the granitoid and pelitic rocks (Aikman and Harrison, 2011); no zircons were recovered from the mafic units. Large, fresh samples were crushed in a mechanical jaw crusher and processed to powder in a tungsten carbide mill, taking considerable care to avoid contamination.

2.2. Bulk rock geochemistry

Major elements were analyzed in lithium borate discs by X-ray fluorescence (XRF) using a Phillips PW2400 spectrometer. Trace elements were analyzed on glass discs using an Agilent 7500S quadrupole inductively-coupled plasma mass spectrometer (ICP–MS) coupled to a 193 nm ArF excimer laser with an 80 μm spot. For LA–ICP–MS analyses, each unknown was measured three or four times and a weighted average of the results taken. Data reduction and limit-of-detection calculations are described in Longerich et al. (1996). Analytical precision and accuracy of LA–ICP–MS measurements were monitored through multiple ablations of BCR-2G and results reproduced the published values (Norman et al., 1998) to within 10% percent in virtually all cases, and typically to within 5%.

2.3. Rb–Sr and Sm–Nd isotopic analysis

Rb–Sr and Sm–Nd isotopic measurements were undertaken using the methods of Gingele and De Deckker (2005) with the exception that samples were digested in Teflon bombs after spiking for isotope dilution. We calculated the Rb concentrations for the Yala-Xiangbo granitoids and Dala granitoids sample suites from trace element analyses using a method (Aikman, 2007) tested on data from the Arunachal leucogranites and Tsona leucogranites suites, for which isotope dilution $^{87}Rb/^{86}Sr$ ratios were obtained (the methods reproduced within uncertainty).

3. Results

Bulk-rock geochemical data for 41 samples, and Rb–Sr and Sm–Nd isotopic data from 28 samples, are given in six tables in the Supplementary Online Material (SOM). As a reference, we compare our results to published data from the Gangdese Batholith granitoids, particularly those close to the Tibetan town of Zedong north of our study area (Debon et al., 1986; Harrison et al., 2000), which are probably representative of concomitant arc magmatism along the southern margin of Eurasia.

3.1. Major elements

The granitoid samples have a relatively restricted range of SiO_2 (70–75%). The Dala granitoids (SOM Table 2) form a tight cluster within the granodiorite field (Streckeisen and Le Maitre, 1979), although one more mafic outlier plots within the quartz-monzodiorite field (Aikman, 2007). The Arunachal leucogranites, Tsona leucogranites and Yala-Xiangbo granitoids (SOM Tables 1 and 3) are more compositionally heterogeneous, scattering among the granodiorite, monzo-granite and quartz-monzonite fields (Aikman,

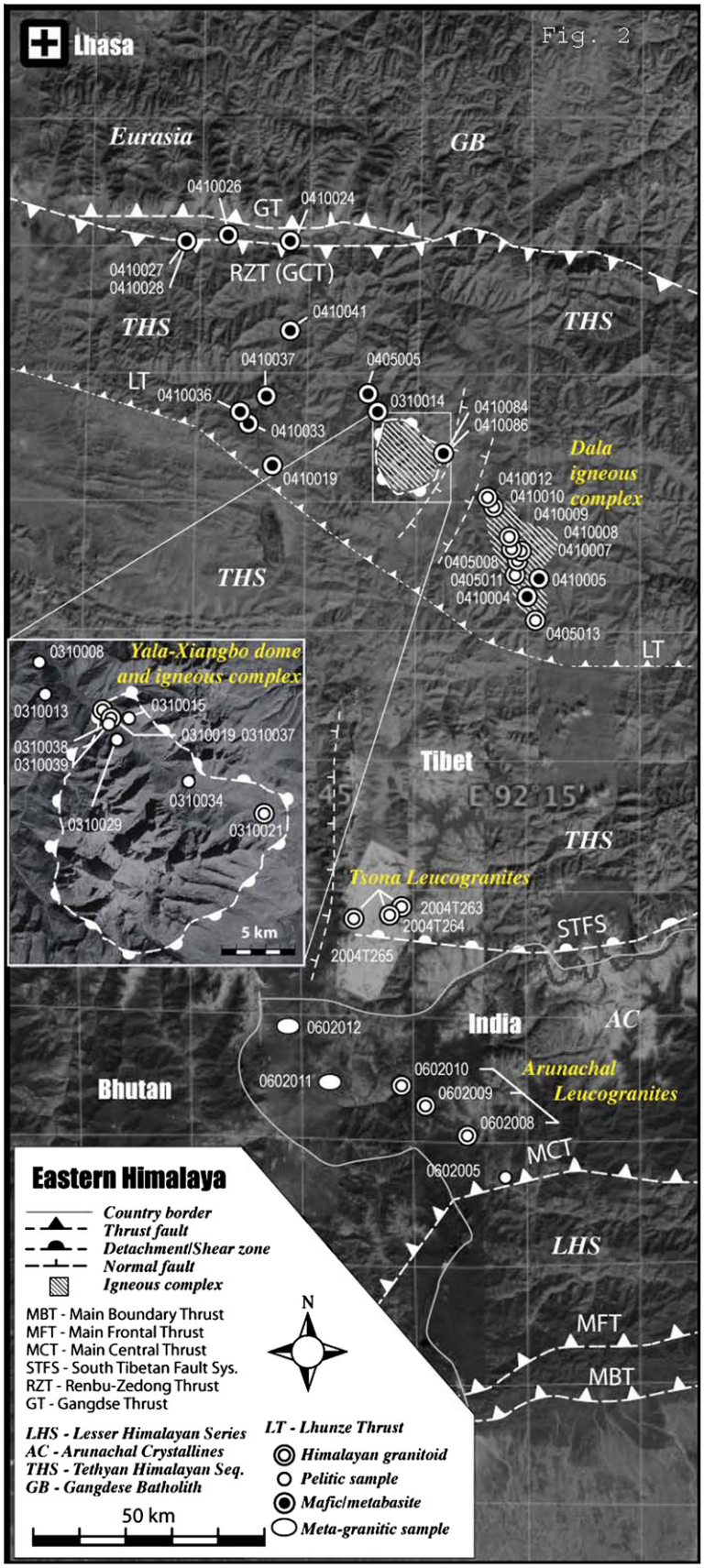

Fig. 2. Schematic geological map of the eastern Himalaya showing the principal tectonic features and sample locations. Map compiled from Yin et al., 1994; Harrison et al., 2000; Pan et al., 2004; Yin, 2006; Aikman, 2007; Aikman et al., 2008.

Table 1
Details of sample suites analyzed for bulk geochemical and isotopic composition. Age data derived from zircon U–Pb geochronology (Aikman et al., 2008, 2012), sample locations as shown in Fig. 2. The ages of the Tethyan mafic bodies are unknown as U–Pb dating proved unsuccessful (no zircons were found). Analyses conducted: major element XRF (M), trace element LA-ICPMS (T), TIMS Rb–Sr & Sm–Nd isotopes (I).

Sample	Lithology	Analysis	Age/notes
Arunachal leucogranites			
602,008			
602,009			
602,010	Leucogranite	MTI	Crystallization at 20.2 ± 2.0 Ma
Tsona leucogranites			
2004T263			
2004T264			
2004T265	Leucogranite	MTI	Crystallization at 18.8 ± 1.2 Ma
Yala-Xiangbo leucogranites			
310,019		MTI	Recrystallized ca. 20 Ma; inferred Eocene cryst.
310,021			Crystallization 42.3 ± 4.9 Ma
310,037	Leucogranite		Recrystallized ca. 20 Ma; inferred Eocene cryst.
310,038			Crystallization 42.3 ± 4.9 Ma
Data granitoids			
405,008	Granodiorite		
405,011	Granodiorite		
405,013	Granodiorite		
410,007	Monzodiorite	MTI	Emplacement and crystallization at 44.1 ± 1.2 Ma
410,008	Granodiorite		
410,009	Granodiorite		
410,010	Granodiorite		
410,012	Granodiorite		
Arunachal crystallines			
602,005	Pelite		Dominantly proterozoic detrital ages
602,011	Metagranite	MTI	Protolith ca. 824 Ma
602,012	Orthogneiss		Protolith ca. 824 Ma
Yala-Xiangbo pelites			
310,008			Inferred triassic depositional age
310,013			Inferred triassic depositional age
310,015			Triassic and older detrital ages
310,029	Pelite	MTI	Triassic and older detrital ages
310,034			Dominantly ordovician detrital ages
310,039			Ordovician and older detrital ages
Tethyan mafics			
410,004		MT	
410,019		MT	
410,024		MT	
410,026		MT	
410,027		MT	
410,028		MT	
410,033		MT	
410,036		MT	
410,037	Mafic	MT	Unknown age
410,041		MT	
405,005		MT	
410,005		MT	
410,084		MT	
410,086		MT	
310,014		MTI	

2007). The two granitic Arunachal crystallines samples (0602011 and 0602012) plot close to the Tsona leucogranites in the monzo-granite field (Zhimithang gneiss) and are distinct from all other sample suites in the alkali-feldspar granite field. The granitoid samples plot predominantly along the high-K calc-alkaline series trend (SOM Fig. 1a), with all but the Yala and Tsona granitoids in the magnesian field of an Fe* diagram (Frost et al., 2001; SOM Fig. 1b). All the suites show relatively high alkali contents (SOM Fig. 3a) with Na/K close to unity (SOM Tables 1–4). None of the four suites shows significant correlation between major elements and silica content (Aikman, 2007).

Most of the granitoid samples analyzed in this study are peraluminous, whereas the Gangdese granitoids are almost exclusively metaluminous (Fig. 3). The Dala granitoids, Arunachal leucogranites, Tsona leucogranites, Yala-Xiangbo granitoids, and Gangdese granitoids plot collectively along a calc-alkaline trend in an AFM diagram (SOM Fig. 3). All but one of the Dala granitoids samples is consistent with minimum melt compositions at high water activities and a range of pressures (Fig. 4). The Arunachal and Tsona leucogranites and Yala-Xiangbo granitoids do not cluster around minimum melt compositions (Fig. 4), reflecting greater variability in major phase abundance.

3.2. Rare earth elements

Rare earth element (REE) patterns, normalized to average C1 chondrites (McDonough and Sun, 1995), are generally consistent within groups. The Gangdese granitoids (Zedong) are consistently LREE enriched (La_N = 150–250) and show negatively sloping trends ($(La/Yb)_N$ = 19–45, $(La/Sm)_N$ = 4.4–8.3) with no discernible Eu anomaly; HREE are typically flat or slightly decreasing (Yb_N = 5.3–8.7, $(Gd/Yb)_N$ = 1.9–3.3) (Fig. 5a). The Dala granitoid REE patterns are almost indistinguishable; the only notable

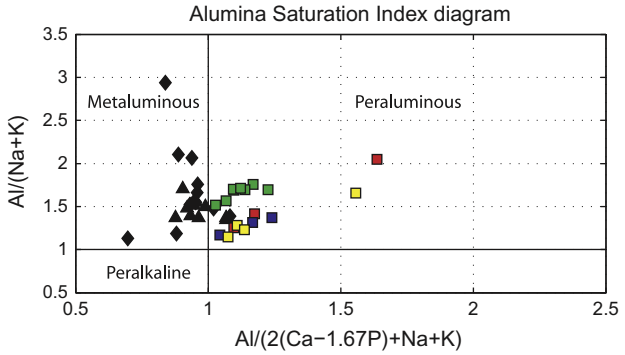

Fig. 3. Alumina Saturation Index diagram for the major-element composition of the Gangdese Batholith granitiods (GB; Debon et al., 1986; Harrison et al., 2000), Yala-Xiangbo granitoids, Dala granitoids (DGs) and Tethyan mafic bodies (TM).

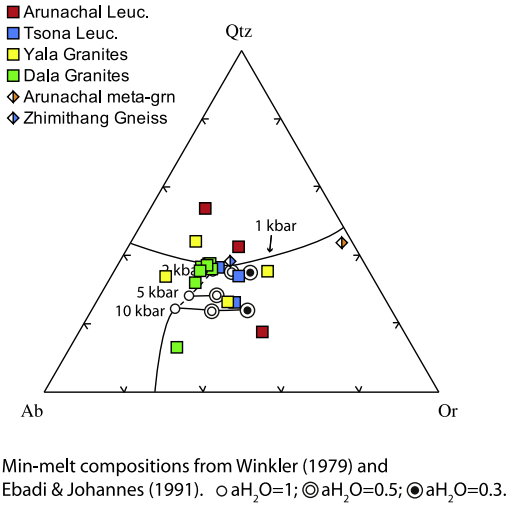

Fig. 4. Ternary phase diagram in the system Quartz–Albite–Orthoclase ± H_2O ± Anorthite showing major element compositions of Gangdese Batholith granitiods (GB; Debon et al., 1986; Harrison et al., 2000), Yala-Xiangbo granitoids, Dala granitoids (DGs) and Tethyan mafic bodies (TM).

difference being their slightly lower HREE enrichment (Yb_N = 2.9–4.9) (Fig. 5a).

The Arunachal and Tsona leucogranites (Fig. 5b) show more variable REE patterns with uniformly decreasing trends (Arunachal leucogranites $(La/Yb)_N$ = 16.7–24.9, Tsona leucogranites $(La/Yb)_N$ = 6.6–22.2) and negative Eu anomalies, but are generally similar to the HHL (e.g., Inger and Harris, 1993; Zhang et al., 2004a). The Yala-Xiangbo granitoids (Fig. 5c) are depleted in LREE with respect to other granitoid samples (La_N = 10.3–35.9) and show two trends: the first similar to Tsona leucogranites, with large Eu anomalies, and the second is comparatively enriched in HREE (Yb_N = 6.7–31.8).

The mafic samples (Fig. 5d; SOM Tables 4 and 5) exhibit a range of REE patterns varying from horizontal to slightly positive or slight negative slopes ($(La/Yb)_N$ = 0.3–6.3). Excluding a single anomalous trend, which is derived from an altered ultramafic cumulate that plots below chondrite, they show depleted LREE (La_N = 1–125) and enriched HREE (Yb_N = ~5–45) with respect to the Gangdese Batholith.

3.3. Trace elements

Granitoids from all sample suites show trace element patterns characterized by incompatible element (LILE) enrichment relative to High Field Strength (HFSE) and REE elements (Fig. 6 normalized to primitive mantle concentrations of McDonough and Sun, 1995; see SOM Tables 1–5). All samples show limited Nb-Ta fractionation almost certainly reflecting Ta contamination during sample preparation using a tungsten carbide mill. The Gangdese granitoids (Harrison et al., 2000) are characterized by tightly bunching trends showing LILE and LREE enrichment, positive Pb anomalies and negative Ba, Nb, Ta, P, Sm and Ti anomalies; Th/U ratios range from 0.9 to 2.2 (Th_N = 170–450, U_N = 150–450). Samples of the Dala granitoids (Fig. 6a) show trace element patterns that are almost indistinguishable from those of the Gangdese granitoids. Pb is slightly higher and the Ba and Sr are slightly lower than the Gangdese granitoids. Trace element patterns from the mafic samples are highly variable (Fig. 6d). They do not show the characteristic LILE enrichment that is present in the Gangdese granitoids and are unlikely to be related. Metamorphosed samples of that suite are not distinguishable from their igneous counterparts in terms of trace element composition.

The Arunachal and Tsona leucogranites and Yala-Xiangbo granitoids (Fig. 6b and c) display significantly more inter-sample heterogeneity than either the Dala or Gangdese granitoids, with similar trace element patterns distinguishable by relatively stronger depletion in Ba, Sr, Zr, Ti and LREE, and a more pronounced positive spike in Pb with respect to the Dala and Gangdese granitoid trends. The trace element patterns are very similar to those of other HHL and NHG (Inger and Harris, 1993; Zhang et al., 2004a).

Crystalline samples from the Arunachal Himalaya (numbered in Fig. 6b) show typical upper crustal trace element patterns. Gneiss sample 0602005 has a high SiO_2 content, is depleted in K and enriched in Zr and Hf, consistent with a detrital sediment rich in quartz and zircon. Sample 0602011 shows distinctive strongly negative Sr and P anomalies. Sample 0602012 shows smaller Ba and Pb excursions and flatter HREE patterns. Overall, these samples are characteristic of the GHC (Inger and Harris, 1993). The Yala-Xiangbo pelites (YPs) trace element patterns (Fig. 6c) are similar to those of other North Himalayan Crystallines (NHCs gneiss and schist, Fig. 6h) and the GHC (Fig. 6g). The comparison between the trace element patterns of the leucogranite and crystalline samples provides some evidence for the trace element redistribution during partial melting. The leucogranites are enriched in Pb, Rb and K, and depleted in Sr and Ba, with respect to the crystalline samples. Generally, LREE, Zr, and Ti are depleted in the leucogranites.

3.4. Rb–Sr and Sm–Nd isotopic analysis

Rb–Sr and Sm–Nd isotopic analyses (Fig. 7; SOM Table 6) reveal a smaller range of initial $^{143}Nd/^{144}Nd$ (0.51178–0.51293) relative to $^{87}Sr/^{86}Sr$ (0.70803–0.87676). Initial Nd isotopic ratios for the Arunachal leucogranites and Tsona leucogranites show consistently negative ε_{Nd} (−13 to −15) with variable ε_{Sr} (+750 to +1700). The range of ε_{Nd} values for the Yala-Xiangbo granitoids is slightly greater (−8 to −13) while ε_{Sr} is relatively primitive (+150 to +350). The Dala granitoids show a restricted range of ε_{Nd} (−10 to −13) with relatively primitive ε_{Sr} (+115 to +170). High-grade Arunachal lithologies have similar ε_{Nd} to Arunachal and Tsona leucogranites (−12 to −16), but a notably greater range of ε_{Sr} (+670 to >2500). Pelitic units from the core of the Yala-Xiangbo dome typically show ε_{Nd} in the range −6 to −8, although one sample (0310034) has a significantly more negative value of ca. −13. The calculated ε_{Sr} from the pelitic samples is also relatively primitive (+150 to +350), excluding the anomalous sample.

Rb/Sr ratios in the Arunachal leucogranites are ~1.5, comparable to two samples of the Arunachal crystallines (0602005, 0602012). Rb/Sr ratios in the Tsona leucogranites are higher (6–12) and nearly overlap the Yala-Xiangbo granitoids and pelites

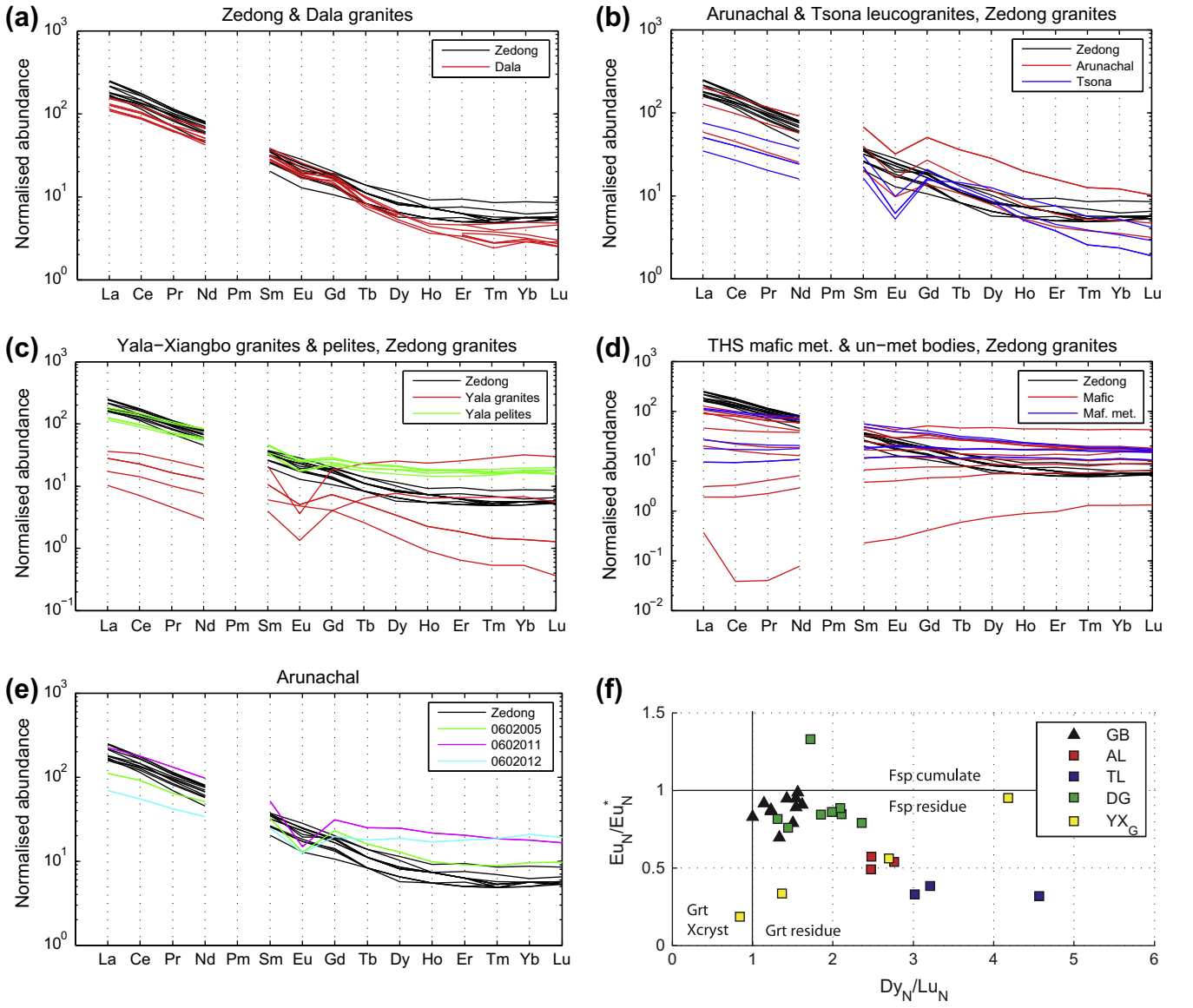

Fig. 5. Chondrite normalized REE diagrams for: (a) Dala granitoids; (b) Arunachal and tsona leucogranites; (c) Yala-Xiangbo granitoids and pelites; (d) Tethyan mafic bodies; (e) Arunachal crystallines. Gandese batholith trends (labeled Zedong; Harrison et al., 2000) are shown for comparison; (f) Shows discrimination diagram plotting expected fields for samples containing cumulus feldspar or feldspar in the residue, and xenocrystic garnet or garnet in the residue.

(1–9 and 0.7–4, respectively). Rb/Sr ratios for the Dala granitoids are consistently 0.2–0.5.

4. Discussion

The major element geochemistry of eastern Himalayan granitoids broadly distinguishes them into two groups. The Dala and Gangdese granitoids are typically calcic-alkalic metaluminous to weakly peraluminous, show broad variations in major elements with SiO_2 consistent with a generalized differentiation trend, and plot at pressure-dependent eutectic compositions. The Arunachal and Tsona leucogranites form a second group that is more variable in terms of major elements. They show no appreciable correlation between major elements and SiO_2, have variable alkali contents, are moderately to strongly peraluminous and have bulk compositions not necessarily consistent with minimum melt compositions. The Yala-Xiangbo granitoids appear superficially similar to the Arunachal and Tsona leucogranites, but their possibly more complex origins are discussed in more detail below.

4.1. Petrogenesis of the dala granitoids

The Dala granitoids plot, along with those from the Gangdese Batholith, in the volcanic-arc granite field of the trace element discrimination diagram of Pearce et al. (1984). Field relations indicate emplacement at shallow crustal levels (Aikman et al., 2008), consistent with crystallization at water-saturated conditions between 1 and 3 kbar (Fig. 4). The Dala granitoids crystallized at 44.1 ± 1.2 Ma (Aikman et al., 2008; Zeng et al., 2011), concomitant with widespread magmatic activity in the Gangdese Batholith (Debon et al., 1986; Harrison et al., 2000). The coincidence and geochemical similarities between the Dala granitoids and Gangdese Batholith samples suggests a petrogenetic link. Although the major element characteristics of the Dala and Gangdese granitoids are consistent with magma differentiation along a liquid line of descent towards the water-saturated granite eutectic, the absence of a pronounced Eu anomaly (Fig. 5a) suggests they formed by mixing of mafic and crustally-derived material (e.g., Debon et al., 1986; Mo et al., 2006). Mafic magmas formed in association with north-dip-

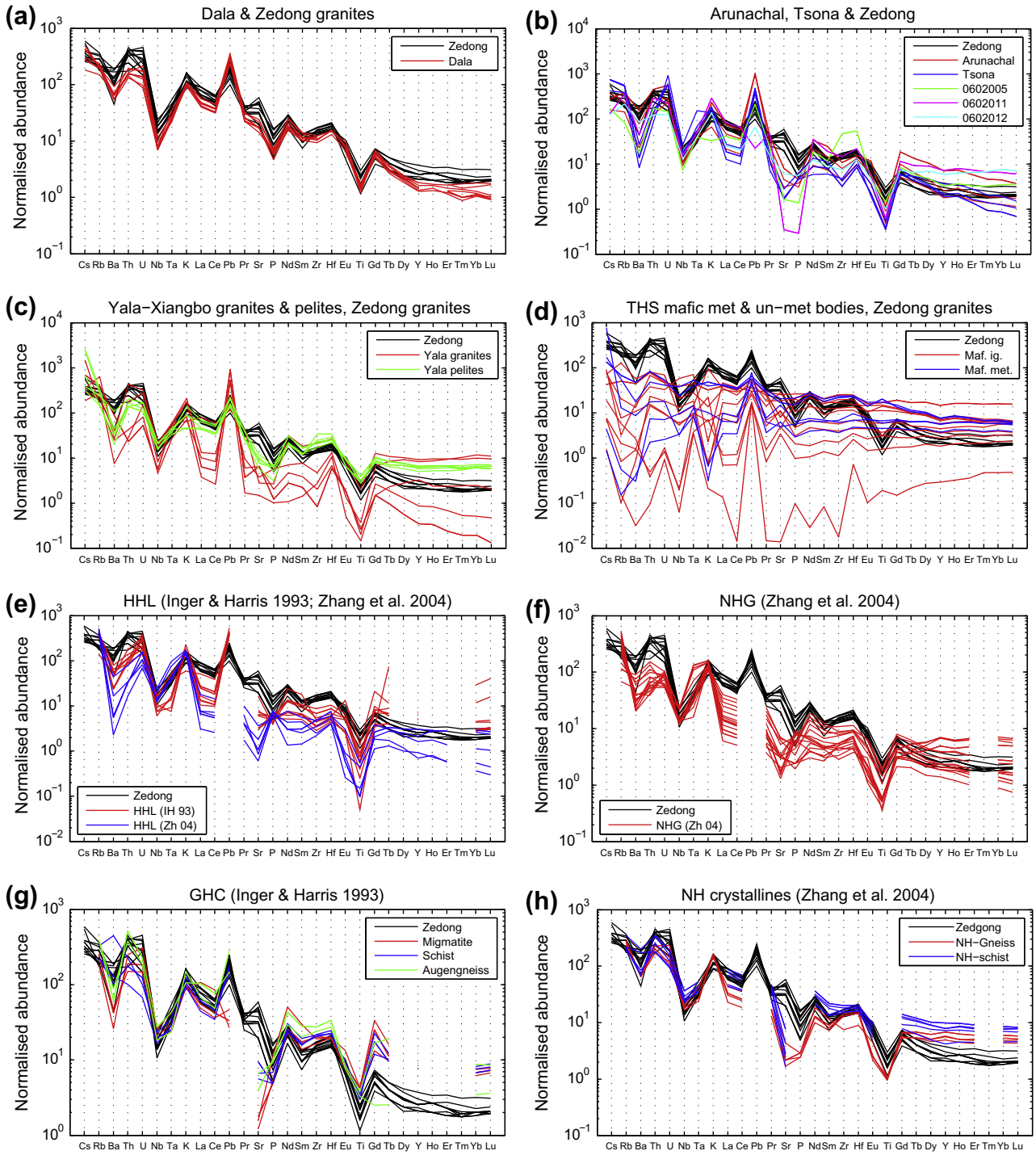

Fig. 6. Primitive mantle normalized spider diagrams for all sample suites, shown with published data from the Gandese Batholith (labeled Zedong; Harrison et al., 2000): (a) Dala granitoids; (b) Arunachal and Tsona leucogranites; (c) Yala-Xiangbo granitoids and pelites; (d) Tethyan mafic bodies; (e–h) show data for the High Himalayan Leucogranites, North Himalayan Granites, Greater Himalayan Crystallines and North Himalayan Crystallines (Inger and Harris, 1992; Zhang et al., 2004a).

ping oblique subduction of Neotethyan oceanic crust, whereas the felsic component was probably young crustal-material derived from the accretionary wedge (Debon et al., 1986; Mo et al., 2006). The bulk geochemical characteristics of the Dala granitoids are consistent with such processes, and their Sr isotopes support a relatively primitive source. However, the Dala granitoids also show comparatively negative ε_{Nd}, pointing to a component of more evolved and quite old crustal material. This suggests the felsic component in the Dala granitoids might be derived from partial melts of crystalline basement.

We constructed isotopic mixing-models between various mafic and crustal end-members in order to assess the suitability of potential source materials for the Dala granitoids. Fig. 8 shows time-corrected (44 Ma) mixing grids, constructed between the inferred isotopic range of the eastern Gangdese Batholith (Mo et al., 2006), and the median isotopic composition of various crustal

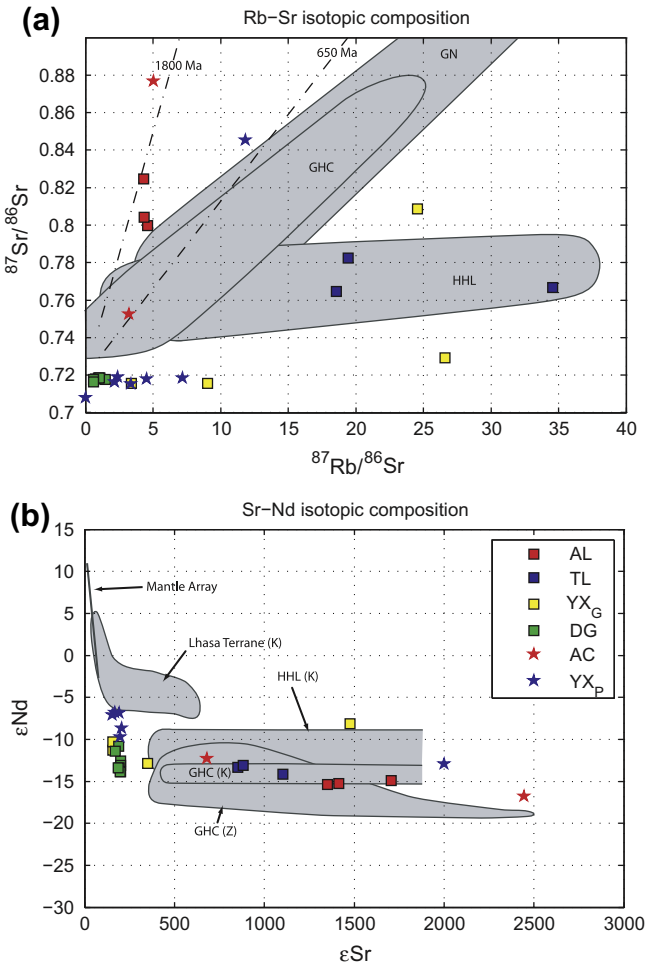

Fig. 7. Rb–Sr and Nd–Sr isotope diagrams: (a) Rb–Sr diagram showing data from the Arunachal and Tsona leucogranites (Arunachal leucogranites, Tsona leucogranites), Dala and Yala-Xiangbo granitoids (DGs, Yala-Xiangbo granitoids), Arunachal crystallines (ACs) and Yala-Xiangbo Pelites (YPs); (b) Nd–Sr diagram showing data from this study and inferred range of isotopic compositions of the GHC, HHL and Lhasa Terrane; (K) denotes fields after Kapp et al. (2005) and (Z) denotes fields after Zhang et al. (2004a,b).

end-members. Samples of mafic bodies from the Tethyan Himalaya (see above) bear no obvious geochemical similarity to either the Dala granitoids or Gangdese Batholith, and their field relations suggest they pre-date Himalayan orogenesis (Aikman, 2007).

Fig. 7a and b shows the possible range of isotopic compositions produced by mixing between Gangdese Batholith and Yala-Xiangbo pelites, and Gangdese Batholith and THS end-members. Mixtures of Gangdese granitoids and Yala-Xiangbo pelites cannot fully account for the observed range of Dala granitoids isotopic compositions. Fig. 7c and d shows mixing grids constructed, respectively, between the Gangdese Batholith and GHC, and the Gangdese Batholith and Inner Lesser Himalaya (ILH; Richards et al., 2005). The isotopic compositions of the Dala granitoids samples lie within the range predicted for mixing between Gangdese Batholith-type mafic magmas and either of the GHC or ILH crustal end-members.

The GHC is widely cited as the basement to the Tethyan Himalaya, whereas the LH series is exposed in the frontal parts of the range (LeFort, 1996; Yin, 2006). While high pressure Eohimalayan GHC metamorphism may have occurred as early as 45 Ma (see LeFort, 1996), post-collisional metamorphism of the Lesser Himalaya is largely associated with Miocene and younger movement on the MCT (LeFort, 1996). Thus, roughly equal parts of GHC and Gangdese material are the most likely source for the Dala granitoids. The one caveat is that since parts of the THS sequence are isotopically indistinguishable from the GHC (Ahmad et al., 2000; Myrow et al., 2003; Richards et al., 2005), a contribution from these units is also possible. We also note the ages of inherited zircons from the Dala granitoids span from 300 to 1800 Ma, with a marked peak at 500 Ma (Aikman et al., 2008). The same peak at 500 Ma is also present in the Tsona leucogranites and granites of the Yala-Xiangbo dome (Aikman, 2007), indicating that all these felsic intrusions involve at least partly a similar crystalline source. It has been recently proposed, based on trace element and isotope data, that the Dala granites might represent partial melts of a thickened mafic lower crust (Zeng et al., 2011). However, the widespread presence of inherited zircons in the Dala granites, their relatively high K_2O contents and the absence of trondhjemites and tonalites in the granite are difficult to reconcile with this hypothesis.

The recognition of Eocene Gangdese-type magmatism in the central Tethyan Himalaya places new constraints on the structural evolution of the Himalayan fold and thrust Belt – for example in terms of the distribution of source and host materials and the latter's subsequent history – and indeed for Himalayan evolutionary models generally. Emplacement of these bodies was concomitant with upper-amphibolite facies metamorphism and formation of the Yala-Xiangbo granitoids (Aikman et al., 2012; Zeng et al., 2011), and a major phase of mantle-derived magmatism in the Gangdese Batholith ~120 km to the north (Debon et al., 1986; Harrison et al., 2000; Mo et al., 2006). Aikman et al. (2012) argued that an extension of the Ninety East Ridge may have been responsible for Eocene high heat-flow beneath the eastern Himalaya and explain the localization of magmatism there at ca. 44 Ma. Their argument is supported by the presence of fractionated Eocene basaltic volcanics in the Siang window in the frontal Himalaya (Sengupta et al., 1996).

4.2. Petrogenesis of the Arunachal and Tsona leucogranites, and Yala-Xiangbo granitoids

The geochemistry of HHL from northern Nepal, and several NHG from southern Tibet, have led previous workers to argue that both granitoid belts formed by melting of the underlying GHC pelitic lithologies during Neohimalayan metamorphism (LeFort et al., 1987; Harris and Inger, 1992; Inger and Harris, 1993; Guillot and LeFort, 1995; Harrison et al., 1997; Yin and Harrison, 2000; Zhang et al., 2004a). The Arunachal leucogranites and Tsona leucogranites geochemistry strongly support their inferred origin as anatectic melts, as they show incompatible element enrichments, high Alumina Saturation Index (ASI), radiogenic enrichments, and relative HFSE depletions that are characteristic of intracrustally-derived granitoids (Harris et al., 1986). The Tsona leucograinte samples are relatively homogeneous, and local variations in pressure and fluid availability during melting can account for their compositional variability (Fig. 4). Extensive fractional crystallization is not favored for the HHL due to mechanical and petrographic arguments (see Inger and Harris, 1993), thus incorporation of cumulus phases in any of the felsic granitoid samples is unlikely. Incomplete magma-crystal separation and limited entrainment of restitic phases are possible, but, in the case of the Arunachal leucogranites, extensive incorporation of either restitic/cumulus feldspar, or xenocrystic garnet, is ruled out by the moderate to strongly negative Eu anomalies (cumulus feldspar would likely produce a positive anomaly) and decreasing normalized HREE patterns shown by all samples (xenocrystic garnet would likely lead to HREE enrichment). Thus, we conclude the Arunachal samples are probably broadly representative of melt compositions, and the observed compositional range of these bodies likely reflects differences in

source-rock compositions (Nabelek et al., 1992; Inger and Harris, 1993), degree of melting and water pressure (Patino Douce and Beard, 1996; Patino Douce and Harris, 1998), together with possible mixing between melts in at least one sample (see below).

The geochemistry of Yala-Xiangbo granitoids is broadly consistent with derivation from crustally-derived melts, and such intracrustal melting has been widely proposed for other NHG (e.g. Harrison et al., 2007; Yin and Harrison, 2000; Zhang et al., 2004a, and references therein). However, because they are isochoronous with the nearby Dala granitoids and granitoids from the Gangdese Batholith, and because amphibolites and mafic enclaves have been documented in the core of the Yala-Xiangbo dome (Aikman, 2007), we consider a hybrid origin for the Yala-Xiangbo granitoids equally plausible. Indeed, it is possible that central parts of the Yala-Xiangbo complex represent fractionated equivalents of the Dala granitoid suite, while some sill and dyke networks around its fringes (Aikman, 2007) constitute partial melts of nearby sediments.

4.3. Source characteristics

We used the isotopic compositions of the Arunachal and Tsona leucogranites and Yala-Xiangbo granitoids to assess possible source regions. GHC sequences of the central and western Himalaya typically plot along a Rb–Sr isochron of ca. 480 Ma (Fig. 7a), and show ε_{Nd} of ca. −15 and ε_{Sr} in the order of 500–2000 (Deniel et al., 1987; Ahmad et al., 2000; Myrow et al., 2003; Richards et al., 2005; Fig. 8a). The HHL typically plot along a ca. 20 Ma Rb–Sr isochron that intersects the GHC field close to initial values (Deniel et al., 1987; Inger and Harris, 1993; Miller et al., 2001; Stern et al., 1989; Ahmad et al., 2000; Zhang et al., 2004a; Fig. 7b). Measured ε_{Nd} for the HHL is typically −10 to −15; ε_{Sr} is also comparable to the GHC (Fig. 7b).

Zhang et al. (2004a,b) suggested that Cambrian orthogneisses, exposed in the cores of several North Himalayan Domes, are isotopically indistinguishable from upper parts of the GHC sequence. These workers found that the isotopic compositions of several NHG are similar to the HHL. They therefore argued the GHC sequence extends beneath the North Himalaya and fostered both granitoid belts. Our data do not exclude this possibility, but we caution that since parts of the THS are isotopically similar to the GHC (Ahmad et al., 2000; Myrow et al., 2003; Richards et al., 2005), this interpretation is ambiguous.

The Tsona leucogranites lie along a 20 Ma Rb–Sr isochron and fall within the documented isotopic range of other HHL on an ε_{Sr}–ε_{Nd} plot (Fig. 7b). They are therefore consistent with a source material that is isotopically akin to both the mica-schists of the central Himalayan GHC sequence (Inger and Harris, 1993) and components of the Tethyan Himalaya, which are in places isotopically indistinguishable. Aikman et al. (2012) found Tertiary inherited zircon cores in the Tsona leucogranites, suggesting a Tethyan

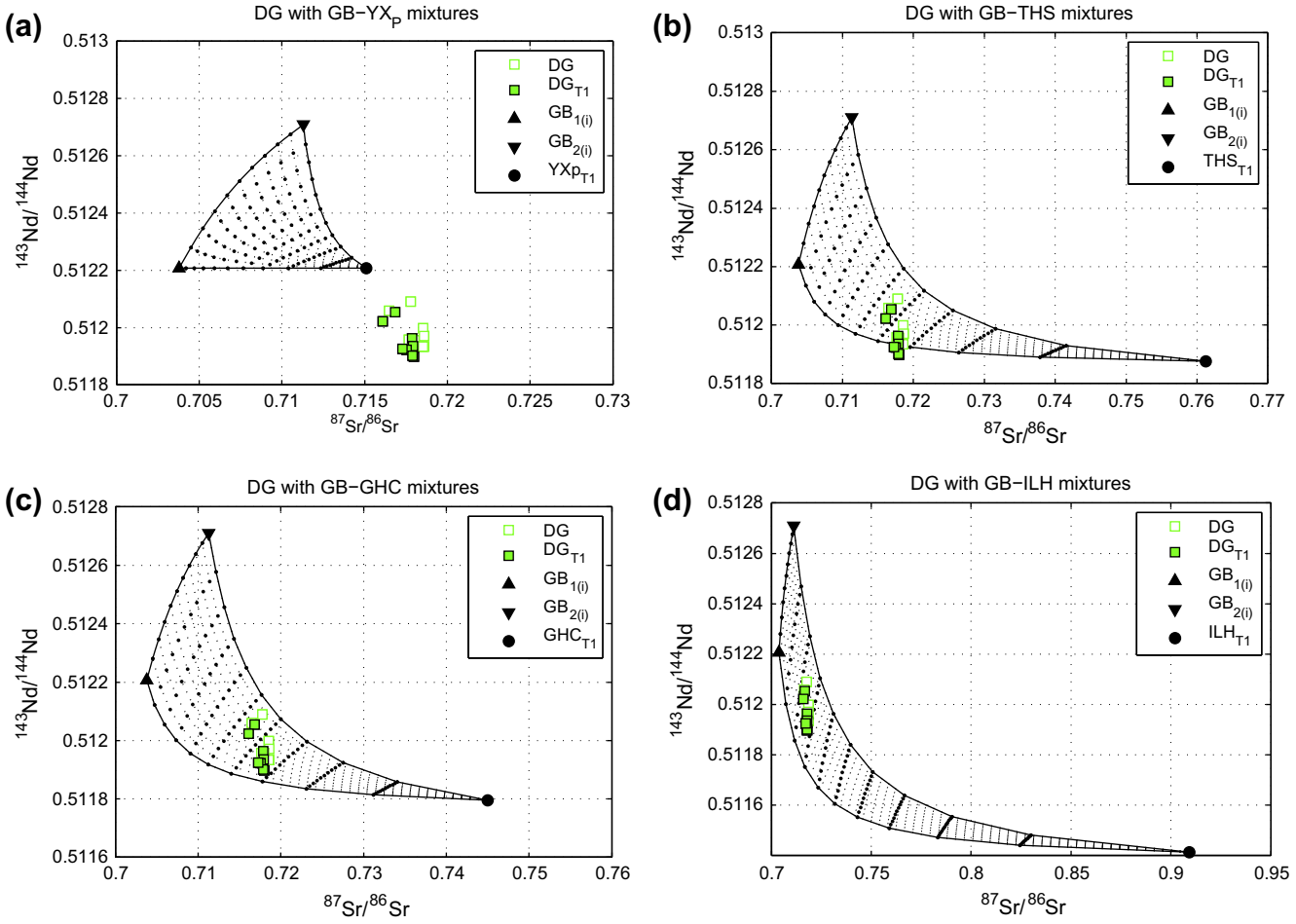

Fig. 8. Isotopic composition of the Dala granitoids (DGs) plotted with mixing models constructed between published data from the Gangdese Batholith (GB) and various crustal end members. $GB_{1,2}$ are end members from a suite of analyses covering the documented range of GB isotopic compositions (Mo et al., 2006). Sialic end member acronyms (YP, GB, THS, ILH) as defined in the text; isotopic compositions taken as median value of the data (Richards et al., 2005; this study). Sub-figure (a) Gangdese Batholith with Yala-Xiangbo pelites; (b) Gangdese Batholith with Tethyan metasediments; (c) Gangdese Batholith with Greater Himalayan Crystallines; (d) Gangdese Batholith with Inner Lesser Himalayan metasediments.

Himalayan source. These few grains, however, could equally well have been acquired by assimilation. Given their structural position close to the STD, and geochemical similarity to other HHL, we suggest a GHC source for the Tsona leucogranites.

The Arunachal leucogranites show generally lower $^{87}Rb/^{86}Sr$ and higher $^{87}Sr/^{86}Sr$ than the Tsona leucogranites and fall outside the documented range of other HHL (Fig. 7a). Together with the Arunachal crystallines, they lie roughly along an 1800 Ma Rb–r isochron—notably older than the GHC isochron. Indeed, the Arunachal leucogranites are isotopically more similar to the Inner Lesser Himalaya (e.g., Ahmad et al., 2000; Myrow et al., 2003; Richards et al., 2005).

Excluding sample 0602011 (an atypical 800 Ma Arunachal meta-granitoid), the Arunachal crystalline sample with the highest (most ILH-like) $^{87}Sr/^{86}Sr$ comes from just above the MCT (Aikman and Harrison, 2011; Fig. 2, sample 0602005). Sample 0602012, from the top of the Arunachal crystallines (Zhimithang gneiss) plots within the established GHC field (Fig. 7a). These data support footwall accretion of material from the Lesser Himalaya, across the MCT; material which subsequently became involved in partial melting to produce leucogranites with similar bulk composition to the central Himalayan HHL. Given the expected behavior of thrust faults to cut up and down section (Suppe et al., 1992), it is not surprising that some material transfer between the footwall and hangingwall of the MCT should occur (Bollinger et al., 2004, 2006). A potential caveat to the footwall-accretion hypothesis is that the presence of <1.8 Ga detrital zircons in the Arunachal crystalline samples (Aikman, 2007) and their ε_{Nd} isotopic composition (Fig. 7b) could preclude them as components of the ILH (Ahmad et al., 2000; Richards et al., 2005). However, since the isotope-defined stratigraphy of the Himalaya sequences is still debated (e.g., Myrow et al., 2003) and recent structural studies have suggested important differences between the Arunachal Lesser Himalaya and that described elsewhere (Yin et al., 2009), such concerns cannot yet be tested.

Samples from the Yala-Xiangbo Dome are isotopically heterogeneous. The data cover an isotopic range that encompasses many other Himalayan units (Fig. 7). Two of the four Yala-Xiangbo granitoid samples are isotopically similar to the YP, with $^{87}Sr/^{86}Sr$ of ca. 0.716 and ε_{Nd} of ca. −10, while the others show higher $^{87}Rb/^{86}Sr$ ratios and $^{87}Sr/^{86}Sr$ closer to the HHL. One anomalous sample from the YP has a significantly more evolved $^{87}Sr/^{86}Sr$ ratio closer to the Cambrian Orthogneiss field of Zhang et al. (2004a). Unfortunately, the isotope-stratigraphy of the THS is insufficiently constrained to definitively identify a source for the Yala-Xiangbo granitoids. However, based on available data and the presence of Triassic inherited-zircon cores (Aikman et al., 2012), the Yala-Xiangbo granitoids probably formed by melting or assimilation of nearby metasedimentary units. The Yala-Xiangbo granitoids appear geochemically distinct from both the Dala granitoids and the various mafic units analyzed, although we cannot exclude the possibility that fractionated equivalents of the Dala granitoid suite are exposed in or buried beneath the inaccessible core of the dome, which includes a ca. 8000 m peak.

4.4. Melting mechanisms

Himalayan petrogenetic models employ a range of mechanisms to produce anatexis (LeFort et al., 1987; Inger and Harris, 1993; Harrison et al., 1998a,b; Beaumont et al., 2001); thus, identifying melting processes can distinguish between these hypotheses. Fluid-present melting of pelites at 5–10 kbar starts at 620–630 °C, whereas under fluid-absent conditions, and equivalent pressures, incongruent muscovite breakdown in "average" pelites begins at ca. 750 °C (Patino Douce and Harris, 1998; cf. 720–760 °C, Peto, 1976; 680–730 °C, Spear, 1995). Incongruent fluid-absent biotite melting begins between 760 °C and 830 °C (Le Breton and Thompson, 1988; Koester et al., 2002), subject to pressure, bulk composition and oxygen fugacity. Methods to assess processeses of granitoid formation mechanisms are generally either *thermometric* or *compositional*. Thermometric techniques (e.g., Harrison and Watson, 1983; Watson and Harrison, 1983, 2005; Rapp and Watson, 1986; Montel, 1993; Watson et al., 2006) infer reactive process by constraining the temperatures of melt formation. Compositional approaches (e.g., Harris and Inger, 1992; Harris et al., 1995; Ayres and Harris, 1997) focus on elemental relationships that are unique to one or more melting reaction.

4.4.1. LILE co-variance

In granites, Rb, Sr and Ba reside in modal phases (micas and feldspars) and thus knowledge of their partition behavior can be used to gain insight into melting reactions (e.g., Inger and Harris, 1993). In the case of fluid-present melting, Harris and Inger (1992) argued that since restite is depleted in feldspar (main host of Sr), the corresponding liquid should be characterized by low Rb/Sr and high Sr/Ba ratios. Fluid-absent melting of muscovite (main host of Rb) will instead increase the proportion of feldspar in the restite resulting in a liquid characterized by high Rb/Sr and low Sr/Ba ratios (Harris and Inger, 1992). Incongruent, fluid-absent

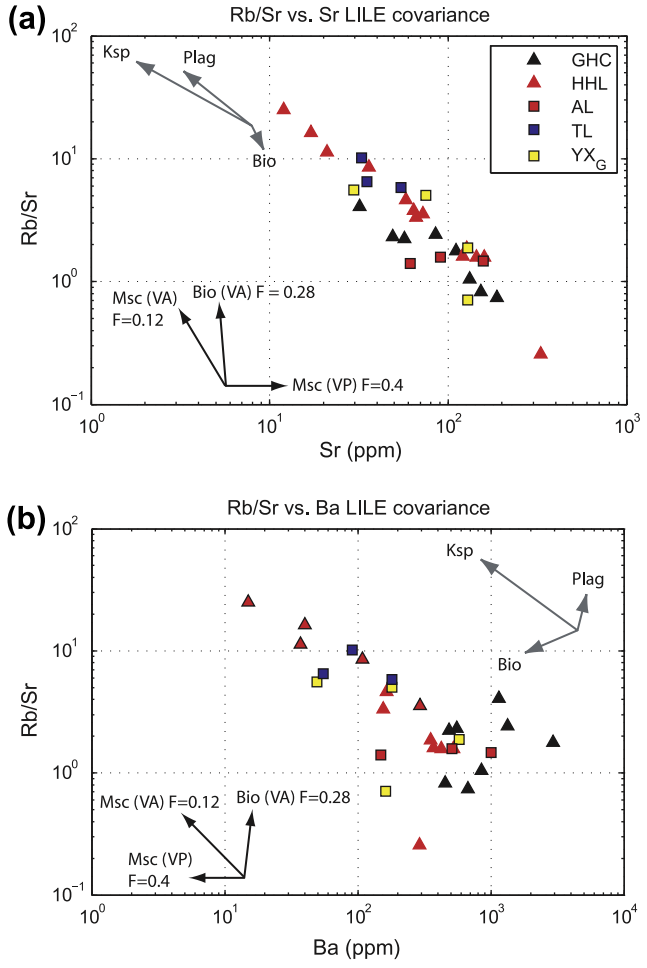

Fig. 9. LILE covariance diagrams showing the Arunachal and Tsona leucogranites (ALs, Tsona leucogranites) and the Yala-Xiangbo granitoids (Yala-Xiangbo granitoids), plotted with published data from the High Himalayan Leucogranites and Greater Himalayan Crystallines (HHL, GHCs; Inger and Harris, 1993; Zhang et al., 2004a). Black vectors show partial melting reactions; gray vectors show 10% crystallization of phases (after Inger and Harris, 1993): (a) Rb/Sr vs. Sr; (b) Rb/Sr vs. Ba.

melting of both muscovite and biotite (i.e., a mica-free restite) is expected to lead to even stronger Rb enrichment.

Fig. 9 shows LILE covariance diagrams for the Arunachal and Tsona leucogranites, Yala-Xiangbo granitoids, HHL, GHC and Arunachal crystallines, plotted with vectors determined by Harris and Inger (1992) for the three melting reactions mentioned above. Note that the HHL appear to define a trend parallel to muscovite fluid-absent melting vector, which has led several previous studies to conclude that they formed by fluid-absent melting of the underlying GHC mica-schists (Harris and Inger, 1992; Inger and Harris, 1993; Zhang et al., 2004a). The Tsona leucogranites plot amongst other HHL, and also follow the fluid-absent melting trend. However, the Arunachal leucogranites have lower Rb/Sr ratios, suggestive of fluid-present melting (Fig. 9). The Yala-Xiangbo granitoids plot amongst other HHL, but do not define a clear trend.

The distinction between fluid-present and fluid-absent melting is also dependent on source composition (i.e., the feldspar to mica ratio) and the amount of water available and thus probably only detectable at high melt fractions (Harris and Inger, 1992). At lower melt fractions, muscovite LILE partitioning must also be considered (cf. Harris and Inger, 1992; Inger and Harris, 1993) and peritectic K-feldspar is likely to influence the LILE systematics of the partial melts (Fig. 9). Thus it is not unambiguously possible to identify the main melting mechanism from LILE covariance diagrams alone. However, the hypothesis that the Arunachal leucogranites were generated by fluid-present melting can be tested with the thermometric data.

4.4.2. Saturation melting temperatures

Zhang et al. (2004a,b) used the LILE co-variance to argue that fluid-absent muscovite melting also produced several of the NHG. They also calculated zircon (T^{sat}_{zir}) and monazite (T^{sat}_{mz}) saturation temperatures (after Watson and Harrison, 1983; Harrison and Watson, 1983; Rapp and Watson, 1986; Montel, 1993) from bulk geochemistry. Despite many of the temperatures being lower than 720 °C, they concluded that fluid-absent melting had dominated.

Fig. 10a shows zircon and monazite saturation melting temperatures for the Arunachal leucogranites, Tsona leucogranites and Yala-Xiangbo granitoids (this study), and the HHL and NHG (Inger and Harris, 1993; Zhang et al., 2004a). The data appear to define two populations, roughly separated by the muscovite fluid-absent melting reaction at 5–10 kbar. The Tsona leucogranites and Yala-Xiangbo granitoids fall in the $\leqslant$720 °C population whereas the Arunachal leucogranites plot with a smaller group between 720 °C and 780 °C.

Even during rapid pelite melting, Zr and LREE contents of melt attain apparent equilibrium with residual zircon and monazite (Acosta-Vigil et al., 2010), thus T^{sat}_{zir} and T^{sat}_{mz} can be used to distinguish between fluid-present melting and muscovite dehydration melting. However, the calculation of a saturation temperature is only feasible as long as zircon and monazite are present in the melted protholith and are accessible for dissolution in the melt. If this is not the case, the resulting temperature represents only a minimum value (Watson and Harrison, 1983). On the other hand, bulk-rock analyses over-estimate the Zr and REE contents of the melt if abundant inherited zircon and monazite are present. Consequently calculated temperatures in such cases overestimate the temperature of melt formation.

In the case of crustal melts, T^{sat}_{mz} is arguably more reliable than T^{sat}_{zir}, since monazite inheritance is less common (Harrison et al., 2002). But the monazite thermometer is susceptible to additional uncertainty in the H_2O content of the melt: the T^{sat}_{mz} given by Zhang et al. (2004a; their Table 1), for example, are only reproducible assuming a nominal water content ($[H_2O]$) of ca. 3%, which may well be too low (all temperatures in Fig. 10 assume $[H_2O] = 8\%$, although any value in the range of 5–11% is probably reasonable; e.g., Holtz et al., 2001).

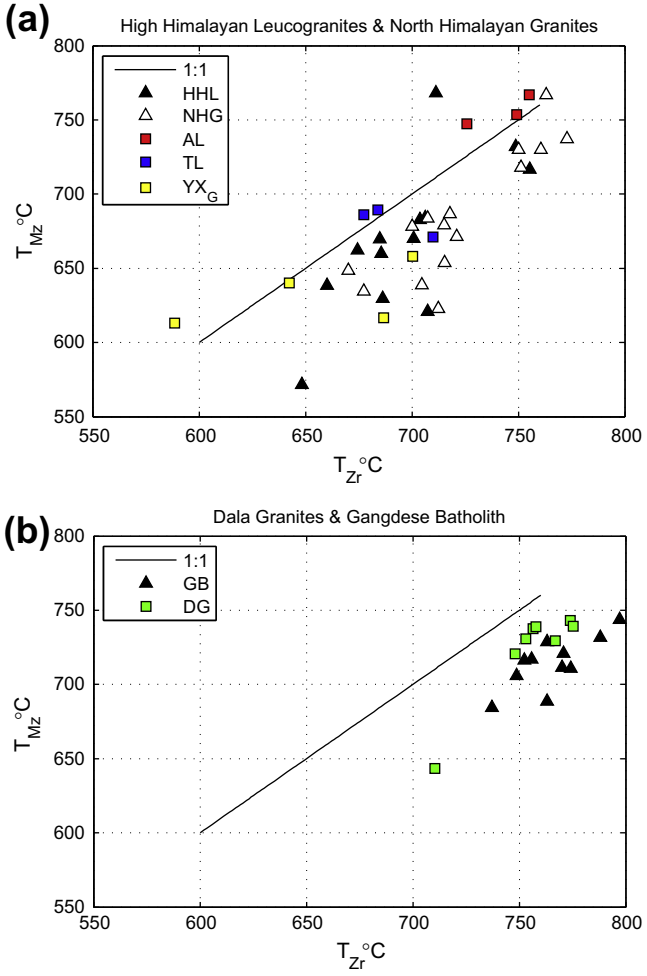

Fig. 10. Zircon and monazite saturation melting temperatures calculated for the Arunachal and Tsona leucogranites (ALs, Tsona leucogranites), and the Yala-Xiangbo and Dala granitoids (Yala-Xiangbo granitoids, DGs). Data from this study are plotted with results calculated for published data from the High Himalayan Leucogranites (HHLs; Inger and Harris, 1993; Zhang et al., 2004a), North Himalayan Granites (Zhang et al., 2004a), and the Gangdese Batholith (Harrison et al., 2000). Monazite saturation melting temperatures assume $[H_2O]$ of 8%. (a) AL, TL, YXG, HHL, NHG; (b) DG, GB.

The saturation temperatures shown in Fig. 10 suggest that many Himalayan granitoids are consistent with formation by fluid-present melting. All HHL and NHG studied to date contain inherited zircon (Harrison et al., 1997 and references therein), and most contain inherited monazite (e.g., Harrison et al., 1995, 1999); thus calculated temperatures are maximum values. Moreover, Harrison et al. (2007) showed that in fractionating plutonic rocks cooling from high-temperature, T^{sat}_{zir} will underestimate the temperature at which zircon begins to crystallize. Hence even this upper-limit may not be robust. Given the aforesaid caveats, we conclude that neither of the methods described above consistently and reliably distinguishes the processes of grantoid formation. However, coupling the Ti-in-zircon thermometer (T_{Ti}, Watson and Harrison, 2005; Watson et al., 2006) with U–Th–Pb dating permits age and crystallization temperature within individual zircon grains to be determined and thus bears on this issue.

4.4.3. Ti-in-zircon thermometry

Ti-in-zircon temperatures for the four investigated suites were reported in Aikman (2007) and Aikman et al. (2012). Here we

discuss the temperature distributions of zircon domains that yielded Alpine ages. The Arunachal and Tsona leucogranite zircons define offset T_{Ti} peaks centered, respectively, at ca. 660 °C and ca. 730 °C (i.e., the reverse of that determined using saturation thermometry; Aikman, 2007; Aikman et al., 2012). In considering whether the apparent T_{Ti} peak offset is robust, we first note that the co-existing rutile in these samples constrains $a_{TiO2} = 1$ and thus underestimation of temperature due to sub-unitiy activites is unlikely. Electron imaging and ion microprobe dating (Aikman et al., 2012) show that the Arunachal leucogranite samples contain significantly more inherited zircon than the Tsona leucogranites, so the apparent offset between the Arunachal leucogranites and Tsona leucogranites T^{sat}_{zir} is due to the high Arunachal leucogranites bulk [Zr]. We estimate that the Arunachal leucogranites samples contain roughly one-third neoformed zircon, compared to at least two thirds in the Tsona leucogranite samples. Hence, the corrected T^{sat}_{zir} for both the Arunachal leucogranites and Tsona leucogranites are within error of each other (in the range 650–680 °C). Indeed, we note that the Arunachal leucogranites T^{sat}_{zir} could plausibly be lower than the Tsona leucogranites if the proportion of inherited zircon is underestimated.

The form of the Tsona leucogranites T_{Ti} distribution (Aikman, 2007; Aikman et al., 2012) conforms to simple theory (Harrison et al., 2007) and the largest T_{Ti} peak in these Zr-saturated magmas should accurately record the temperature of melt formation (Harrison et al., 2007). The obtained temperature peak at 720 °C coincides with the inferred position of muscovite breakdown and hence we ascribe Tsona leucogranite formation to fluid-absent muscovite melting (i.e., consistent with inferences from the LILE plots; Fig. 9).

The Yala-Xiangbo zircon T_{Ti} distribution is probably not a reliable indicator of the temperature of melt formation (Aikman, 2007; Aikman et al., 2012). However other lines of evidence, such as the low saturation temperatures and abundance of tourmaline and pegmatite (Aikman, 2007), suggest at least some parts of the complex formed by fluid-present melting.

The Arunachal leucogranite T_{Ti} distribution is broader than for the Tsona leucogranites, with a dominant peak at ca. 660 °C, and a small shoulder at ca. 730 °C (Aikman, 2007; Aikman et al., 2012). Taken together with the evidence from LILE covariance (Fig. 9), zircon saturation arguments, and the presence of co-existing rutile, we interpret these granitoids to have formed by fluid-present melting close to or at minimum melting conditions. As noted earlier, isotopic data indicate the Arunachal leucogranites were derived from metasediments probably including the Lesser Himalayan sequences. Unlike the GHC, the exposed Lesser Himalayan sequences did not experience widespread Eohimalayan metamorphism (LeFort, 1996; Yin and Harrison, 2000; Celerier, 2007), and thus did not experience previous dehydration reactions. Hence, fluid-present melting appears plausible and likely. It is worth pointing out here that, to our knowledge, the T_{Ti} distribution derived from Alpine-age Arunachal leucogranite zircons (i.e., the peak at ca. 660 °C) is unique among granitoids investigated to date. The zircon temperature spectrum it mostly closely resembles is that for Hadean igneous zircons (with a peak at ~680 °C) for which a similar minimum melting origin has been proposed (see Harrison, 2009).

The inference of Lesser Himalayan material within lower parts of the Arunachal Crystalline sequence is consistent with models predicting footwall accretion during movement on the MCT (e.g., Bollinger et al., 2004, 2006). Furthermore, melting of fertile Lesser Himalayan metasediments explains the occurrence of leucogranites at the base of the Arunachal Crystalline sequence (Yin, 2006; this study), directly above the MCT (cf. in Nepal, where large leucogranites have only been found near the top of the GHC sequence). Melting has been documented in Sikkim (Dasgupta et al., 2009), ~200 km to the west of the Arunachal leucogranites, in MCT zone rocks believed to be part of the Lesser Himalaya. In that prograde metamorphic sequence, both fluid-present and fluid-absent melting reactions are observed. The shoulder on the high-temperature side of the Arunachal leucogranite zircon T_{Ti} peak may reflect zircons formed during fluid-absent melting within the Arunachal GHC sequences proper. Support for this argument is provided by the positions of the dominant T_{Ti} peaks for individual Arunachal leucogranite samples, which increase proportional to increasing structural level (Aikman, 2007; Aikman et al., 2012), as would be expected in an inverted temperature gradient. These data may record a unique snapshot of that inverted gradient – in time, temperature and space – in contrast to a simple metamorphic field gradient.

4.5. Implications

4.5.1. Conditions for fluid-present anatexis

Earlier studies have proposed fluid-present melting of the GHC sequences (not the Lesser Himalayan) to explain formation of the Miocene HHL (e.g. LeFort et al., 1987). Although this model is locally supported by data from NW India (Prince et al., 2001), it has not been favored by workers in the central Himalayan region (Harris and Inger, 1992; Inger and Harris, 1993; Harrison et al., 1997, 1998a,b). Thermal diffusion during MCT slip at a wide variety of rates rapidly yields sigmoidal isotherms (e.g. Harrison et al., 1998a,b; Beaumont et al., 2001; Bollinger et al., 2004). Although early studies struggled to produce sufficient heat to induce anatexis (England et al., 1992), this issue is transcended if slip occurs on a shallowly-dipping or flat ramp that later steepens to form the present-day MCT (Harrison et al., 1998a,b; Beaumont et al., 2001).

Although most dehydration reactions occur during greenschist and lower amphibolite facies metamorphism, continuous H_2O-producing reactions occur up to the onset of anatexis (Spear, 1995). Hence, in the vast majority of scenarios where crustal isotherms close to the "wet" solidus are inverted, the lower temperature portion of the sigmoid can release fluid into the hotter, overlying material, and initiate melting (LeFort, 1975). Furthermore, since the ratio of under- to over-thrusting during MCT motion may have been as high as 3:1 (Bollinger et al., 2004, 2006), development of a persistent inverted geotherm is possible. The supply of fertile material to the melt-zone probably greatly outpaced the rate at which accumulating melt was removed. Since the proportion of melt generated is primarily limited by fluid availability, any such fluid migrating (e.g., by dilatancy pumping, Brown, 1994; McCaig et al., 2000) could locally produce sufficiently high melt-fractions to allow melt migration upon entering the upper plate.

4.5.2. Regional tectonics

Aikman et al. (2008) showed that the principal phase of crustal thickening in the eastern Tethyan Himalaya had terminated by 44.1 ± 1.2 Ma, and our data require a Gangdese-type source beneath Indian Tethyan Himalaya during the Eocene. It is unlikely that the Indian foreland was far-removed from Eurasia during the early Tertiary. While our data do not preclude the presence of a back-arc basin or multiple subduction zones, their simplest explanation places the Tethyan sediments in the hanging-wall of the main Himalayan decollement at ca. 45 Ma, and prevents significant underthrusting of Indian lithosphere at that time (e.g. Replumaz et al., 2004).

Early Himalayan crustal thickening created a north-dipping Tethyan fold and thrust belt (Ratschbacher et al., 1992; Aikman et al., 2008) while arc-magmatism continued in the Gangdese Batholith (e.g., Mo et al., 2006). The Dala granitoids provide the evidence of Eohimalayan arc-like magmatism south of the Indus-

Tsangpo Suture (Aikman et al., 2008; Aikman et al., 2012; Zeng et al., 2011) during amphibolite-grade metamorphism and anatexis at Yala-Xiangbo. Thus the Eohimalayan thermal event extended at least in a N–S direction. Thermochronologic data preclude significant cooling of either the Dala granitoids or the Yala-Xiangbo complex between ca. 45–15 Ma indicating that the eastern Tethyan Himalaya was tectonically quiescent during this interval (Aikman et al., 2012).

To a first order, the Neohimalayan tectonics of the eastern Himalaya appears broadly similar to those described elsewhere: the dominant structural boundaries (MCT, STD, GCT, and various frontal thrusts) controlled the principal movements of heat and mass within the orogen, and magmatism was intimately associated with deformation. Our data suggest that both fluid-absent muscovite dehydration melting of the GHC metasediments, and fluid-present melting of the Lesser Himalayan sequences contributed to the formation of east-Himalayan leucogranites, and that "wet" melting may be a more important mechanism of granite formation there than presently thought.

The apparent spatial and temporal proximity of magmatism with rapid exhumation in several North Himalayan Domes has led some workers to propose a genetic link (Lee et al., 2000, 2004; Beaumont et al., 2001, 2004; Zhang et al., 2004a). However, in the Yala-Xiangbo dome magmatism preceded exhumation by ca. 20 million years, favoring a structural control - probably Miocene north-directed motion on the GCT (Aikman et al., 2012). Associated burial and de-watering of fertile sediments, such as burial of the Xigaze fore-arc sequences that are absent in the eastern Himalaya (Pan et al., 2004), may explain the 20 Ma fluid-mitigated recrystallization event documented at Yala-Xiangbo (Aikman et al., 2012).

5. Conclusions

Post-collisional magmatism along a transect through the eastern Himalaya at ca. 92°E occurred in two modes. The first is represented by Eocene igneous complexes exposed, respectively, in the central Tethyan Himalaya (the Dala granitoids) and in the core of the Yala-Xiangbo dome. The Dala granitoids formed from Gangdese-type magmas that assimilated approximately 50% crustal material from the Greater Himalayan Crystalline (GHC) and/or Tethylan Himalayan Series (THS) sequences during ascent and emplacement at shallow crustal levels. The Yala-Xiangbo granitoids are leucocratic sills, dykes and small plutons that, although structurally similar to the North Himalayan Granites (NHGs), were emplaced ca. 20 m.y. earlier. The second group is represented by anatectic granitoids that are similar to the High Himalayan Leucogranites (HHLs) and NHG. The Miocene Arunachal and Tsona leucogranites crop out, respectively, within the Arunachal GHC adjacent to the South Tibetan Detachment. The Tsona leucogranites appear to have formed by fluid-absent melting of nearby units while the Arunachal leucogranites formed by a combination of both fluid-absent muscovite melting and fluid-present melting of the Lesser Himalayan series. By ~45 Ma, the thickened THS metasediments were already in the hanging wall of the main Himalayan decollement. During the Eohimalayan episode, the eastern Himalaya experienced amphibolite-grade metamorphism and localized, Gangdese-type granitic magmatism; the episode was followed by a period of tectonic quiescence in the north Himalaya, whilst shortening presumably continued further south. The Neohimalayan history of the eastern Himalaya is similar to other parts of the range. Deformation and magmatism were intimately associated in the frontal Himalaya, while exhumation occurred in the North Himalaya due to thrusting along the Indus Tsangpo Suture.

Acknowledgments

Dr. Ulrike Troitzsch is thanked for assistance with XRF analyses, and Dr. Marc Norman for Rb–Sr and Sm–Nd analyses. Charlotte Allen provided technical advice on the acquisition of LA–ICP–MS data. This research was funded by the Australian Research Council and the National Science Foundation. Comments from three anonymous reviewers also improved this manuscript.

Appendix A. Supplementary material

Supplementary data associated with this article can be found, in the online version, at http://dx.doi.org/10.1016/j.jseaes.2012.05.018.

References

Acosta-Vigil, A., Buick, I.S., Hermann, J., Cesare, B., Rubatto, D., London, D., Morgan, G.B.V., 2010. Mechanisms of crustal anatexis: a geochemical study of partially melted metapelitic enclaves and host dacite, SE Spain. J. Petrol. 51, 785–821.

Ahmad, T., Harris, N., Bickle, M., Chapman, H., Bunbury, J., Prince, C., 2000. Isotopic constraints on the structural relationships between the Lesser Himalayan Series and the high Himalayan Crystalline Series, Garhwal Himalaya. Geol. Soc. Am. Bull. 112, 467–477.

Aikman A.B., 2007. Tectonics of the Eastern Tethyan Himalaya. Ph.D. Thesis, The Australian National University.

Aikman, A.B., Harrison, T.M., Lin, D., 2008. Evidence for Early (>44 Ma) Crustal Thickening, Tethyan Hiamalaya, southeastern Tibet. Earth Planet. Sci. Lett. 274, 14–23. http://dx.doi.org/10.1016/j.epsl.2008.06.038.

Aikman, A.B., Harrison, T.M., Herman, J., 2012. Age and thermal history of Eo- and Neohimalayan granitoids, Eastern Himalaya. J. Asian Earth Sci. 51, 85–97.

Ayres, M., Harris, N., 1997. REE fractionation and Nd-isotope disequilibrium during crustal anatexis: constraints from Himalayan leucogranites. Chem. Geol. 139, 249–269.

Beaumont, C., Jamieson, R.A., Nguyen, M.H., Lee, B., 2001. Himalayan tectonics explained by extrusion of a low-viscosity crustal channel coupled to focused surface denudation. Nature 414, 738–742.

Beaumont, C., Jamieson, R.A., Nguyen, M.H., Medvedev, S., 2004. Crustal channel flows: 1. Numerical models with applications to the tectonics of the Himalayan–Tibetan orogen. J. Geoph. Res. 109, B06406.

Bollinger, L., Avouac, J.P., Beyssac, O., Catlos, E.J., Harrison, T.M., Grove, M., Goffe, B., Sapkota, S., 2004. Thermal structure and exhumation history of the lesser Himalaya in central Nepal. Tectonics 23. http://dx.doi.org/10.1029/2003TC001564.

Bollinger, L., Henry, P., Avouac, J., 2006. Mountain building in the Nepal Himalaya: thermal and kinematic model. Earth Planet. Sci. Lett. 244, 58–71.

Brown, M., 1994. The generation, segregation, ascent and emplacement of granite magma – the migmatite to crustally derived granite connection in thickened orogens. Earth Sci. Rev. 36, 83–130.

Celerier, J., 2007. The Thermal And Structural Evolution Of The Kumaun And Garwhal Lesser Himalaya, India. Ph.D. Thesis, The Australian National University.

Chen, Z., Liu, Y., Hodges, K.V., Burchfi el, B.C., Royden, L.H., Deng, C., 1990. The Kangmar dome: a metamorphic core complex in southern Xizang (Tibet). Science 250, 1552–1556.

Dasgupta, S., Chakraborty, S., Sudipta, N., 2009. Petrology of an inverted Barrovian sequence of metapelites in Sikkim Himalaya, India: constraints on the tectonics of inversion. Am. J. Sci. 309, 43–84.

Davidson, C., Grujic, D.E., Hollister, L.S., Schmid, S.M., 1997. Metamorphic reactions related to decompression and synkinematic intrusion of leucogranite, high Himalayan Crystallines, Bhutan. J. Met. Geol. 15, 593–612.

Debon, F., LeFort, P., Sheppard, S., Sonet, J., 1986. The four plutonic belts of the Transhimalaya–Himalaya: a chemical, mineralogical, isotopic, and chronological synthesis along a Tibet–Nepal granite section. J. Petrol. 27, 219–250.

Deniel, C., Vidal, P., Fernandez, A., Lefort, P., Peucat, J.J., 1987. Isotopic study of the Manaslu Granite (Himalaya, Nepal) – inferences on the age and source of Himalayan Leukogranites. Contrib. Mineral. Petrol. 96, 78–92.

Ding, L., Kapp, P., Wan, X., 2005. Paleocene–eocene record of ophiolite obduction and initial India–Asia collision, south central Tibet. Tectonics 24, TC3001. http://dx.doi.org/10.1029/2004TC001729.

England, P., Le Fort, P., Molnar, P., Pecher, A., 1992. Heat sources for Tertiary magmatism and anatexis in the Annapurna–Manaslu region of Central Nepal. J. Geophys. Res. 97, 2107–2128.

Frost, B.R., Barnes, C.G., Collins, W.J., Arculus, R.J., Ellis, D.J., Frost, C.D., 2001. A geochemical classification for granitic rocks. J. Petrol. 42, 2033–2048.

Gingele, F.X., De Deckker, P., 2005. Clay mineral, geochemical and Sr–Nd isotopic fingerprinting of sediments in the murray–darling fluvial system, southeast Australia. Aust. J. Earth Sci. 52, 965–974.

Guillot, S., Lefort, P., 1995. Geochemical constraints on the bimodal origin of High Himalayan leukogranites. Lithos 35, 221–234.

Harris, N.B.W., Pearce, J. A., Tindle, A.G., 1986. Geochemical characteristics of collision zone magmatism. In Collision Tectonics. In: Shakelton, R.M., Ries, A.C., Coward, M.P. (Eds.), Geological Society of London, Spec. Publ., pp. 67–81.
Harris, N., Inger, S., 1992. Trace element modelling of pelite-derived granites. Contrib. Mineral Petrol. 110, 46–56.
Harris, N., Massey, J., 1994. Decompression and anatexis of Himalayan metapelites. Tectonics 13 (6), 1537–1546.
Harris, N., Ayres, M., Massey, J., 1995. Geochemistry of granitic melts produced during the incongruent melting of muscovite – implications for the extraction of Himalayan leukogranite magmas. J. Geophys. Res. 100, 15767–15777.
Harrison, T.M., 2009. The Hadean crust: evidence from >4 Ga zircons. Ann. Rev. Earth Planet. Sci. 37, 479–505.
Harrison, T.M., Watson, E.B., 1983. Kinetics of zircon dissolution and zirconium diffusion in granitic melts of variable water-content. Contrib. Mineral. Petrol. 84, 66–72.
Harrison, T.M., McKeegan, K.D., Lefort, P., 1995. Detection of inherited monazite in the manaslu leukogranite by ^{208}Pb–^{232}Th ion microprobe dating – crystallization age and tectonic implications. Earth Planet. Sci. Lett. 133, 271–282.
Harrison, T.M., Lovera, O.M., Grove, M., 1997. New insights into the origin of two contrasting Himalayan granite belts. Geology 25, 899–902.
Harrison, T.M., Grove, M., Lovera, O.M., Catlos, E.J., 1998a. A model for the origin of Himalayan anatexis and inverted metamorphism. J. Geophys. Res. 103, 27017–27032.
Harrison, T.M., Grove, M., McKeegan, K.D., Coath, C.D., Lovera, O.M., Fort, P.L., 1999. Origin and episodic emplacement of the Manaslu intrusive complex, central Himalaya. J. Petrol. 40, 3–19.
Harrison, T.M., An, Y., Grove, M., Lovera, O.M., Ryerson, F.J., Zhou, X., 2000. The zedong window; a record of superposed tertiary convergence in southeastern Tibet. J. Geophys. Res. 105, 19211–19230.
Harrison, T.M., Catlos, E.J., Montel, J.-M., 2002. U-Th-Pb dating of phosphate minerals. In: Phosphates: Geochemical, Geobiological and Materials Importance, Reviews in Mineralogy and Geochemistry, vol 48. Mineralogical Society of America, Washington, DC, pp. 523–558.
Harrison, T.M., Watson, E.B., Aikman, A.B., 2007. Temperature spectra of zircon crystallization in plutonic rocks. Geology 35, 635–638.
Harrison, T.M., Grove, M., Lovera, O.M., Catlos, E.J., 1998b. A model for the origin of Himalayan anatexis and inverted metamorphism. J. Geophys. Res. 103, 27017–27032.
Holtz, F., Johannes, W., Tamic, N., Behrens, H., 2001. Maximum and minimum water contents of granitic melts generated in the crust: a reevaluation and implications. Lithos 56, 1–14.
Inger, S., Harris, N., 1992. Tectonothermal evolution of the High Himalayan crystalline sequence, Langtang Valley, northern Nepal. J. Metamorph. Geol. 10, 439–452.
Inger, S., Harris, N., 1993. Geochemical constraints on leucogranite magmatism in the Langtang Valley, Nepal Himalaya. J. Petrol. 34, 345–368.
Kapp, J.L.D., Harrison, T.M., Kapp, P.A., Grove, M. Lovera, O.M., Lin, D., 2005. The Nyainqentanglha Shan: A window into the tectonic, thermal and geochemical evolution of the Lhasa block, southern Tibet. J. Geophys. Res. 110, http://dx.doi.org/10.1029/2004JB003330.
King, J., Harris, N., Argles, T., Parrish, R., Zhang, H., 2011. Contribution of crustal anatexis to the tectonic evolution of Indian crust beneath southern Tibet. Geol. Soc. Am. Bull. 123, 218–239.
Koester, E., Pawley, A.R., Luis, A.D., Fernandes, L.A.D., Porcher, C.C., Soliani Jr., E., 2002. Experimental melting of cordierite gneiss and the petrogenesis of syn-transcurrent peraluminous granites in southern Brazil. J. Petrol. 43, 1595–1616.
Le Breton, N., Thompson, A.B., 1988. Fluid-absent (dehydration) melting of biotite in metapelites in the early stages of crustal anatexis. Contrib. Mineral. Petrol. 99, 226–237.
Lee, J., Hacker, B.R., Dinklage, W.S., Wang, Y., Gans, P., Calvert, A., Wan, J.L., Chen, W.J., Blythe, A.E., McClelland, W., 2000. Evolution of the Kangmar Dome, southern Tibet: structural, petrologic, and thermochronologic constraints. Tectonics 19, 872–895.
Lee, J., Hacker, B., Wang, Y., 2004. Evolution of north Himalayan gneiss Domes: structural and metamorphic studies in Mabja Dome, southern Tibet. J. Struct. Geol. 26, 2297–2316.
LeFort, P., 1975. Himalayas, the collided range. Present knowledge of the continental arc. Am. J. Sci. 275 (A), 1–44.
LeFort, P., Vuney, M., Deniel, C., France-Lanord, C., 1987. Crustal generation of the Himalayan Leucogranites. Tectonophysics 134, 39–57.
LeFort, P., 1996. Evolution of the Himalaya. In: Yin, A., Harrison, T. (Eds.), The Tectonics of Asia. Cambridge University Press, pp. 95–106.
Longerich, H.P., Jackson, S.E., Gunther, D., 1996. Laser ablation inductively coupled plasma mass spectrometric transient signal data acquisition and analyte concentration calculation. J. Anal. Atom. Spectrom. 11, 899–904.
McCaig, A., Wayne, D., Rosenbaum, J., 2000. Fluid expulsion and dilatancy pumping during thrusting in the pyrenees: Pb and Sr isotope evidence. Geol. Soc. Am. Bull. 112, 1199–1208.
McDonough, W.F., Sun, S., 1995. The composition of the Earth. Chem. Geol. 120, 223–253.
Miller, C., Thoni, M., Frank, W., Grasemann, B., Klotzli, U., Guntli, P., Draganits, E., 2001. The early palaeozoic magmatic event in the northwest Himalaya, India: source, tectonic setting and age of emplacement. Geol. Mag. 138, 237–251.
Mo, X., Zhao, Z., Deng, J., Flower, M., Yu, X., Lui, Z., Li, Y., Zhou, S., Dong, G., Zhu, D., Wang, L., 2006. Petrology and geochemistry of postcollisional volcanic rocks from the Tibetan Plateau: implications for lithosphere heterogeneity and collision-induced asthenosphere flow. GSA Spec. Paper. 463, 507–530.
Montel, J.M., 1993. A model for monazite/melt equilibrium and application to the generation of granitic magmas. Chem. Geol. 110, 127–146.
Myrow, P.M., Hughes, N.C., Paulsen, T.S., Williams, I.S., Parcha, S.K., Thompson, K.R., Bowring, S.A., Peng, S.C., Ahluwalia, A.D., 2003. Integrated tectonostratigraphic analysis of the Himalaya and implications for its tectonic reconstruction. Earth Planet. Sci. Lett. 212, 433–441.
Nabelek, P.I., Russ-Nabelek, C., Denison, J.R., 1992. The generation and crystallization conditions of the proterozoic harney peak leucogranite, black hills, south Dakota, USA: petrologic and geochemical constraints. Contrib. Mineral. Petrol. 110, 173–191.
Norman, M.D., Griffin, W.L., Pearson, N.J., Garcia, M.O., O'Reilly, S.Y., 1998. Quantitative analysis of trace element abundances in glasses and minerals: a comparison of laser ablation inductively coupled plasma mass spectrometry, solution inductively coupled plasma mass spectrometry, proton microprobe and electron microprobe data. J. Anal. Atom. Spectrom. 13, 477–482.
Pan, G., Ding, J., Yao, D., Wang, L., 2004. Geological map of Qinghai-Xiang (Tibet) plateau and adjacent areas (1:1500,000). China Geological Survey, Chengdu Cartographic Publishing House, Chengdu, China.
Patino Douce, A.E., Beard, J.S., 1996. Effects of P, f_{O2} and Mg/Fe ratio on dehydration melting of model metagreywackes. J. Petrol. 37, 999–1024.
Patino Douce, A.E., Harris, N.B.W., 1998. Experimental constraints on Himalayan anatexis. J. Petrol. 39, 689–710.
Pearce, J., Harris, N., Tindle, A., 1984. Trace element discrimination diagrams for the tectonic interpretation of granitic rocks. J. Petrol. 25, 956–971.
Peto, P., 1976. An experimental investigation of melting relations involving muscovite and paragonite in the silica-saturated portion of the system K_2O–Na_2O–Al_2O_3–SiO_2–H_2O To 15 kb total pressure. Prog. Exper. Petrol. 3, 41–45.
Pinet, C., Jaupart, C., 1987. A thermal model for the distribution in space and time of the Himalayan granites. Earth Plan. Sci. Lett. 84, 87–99.
Prince, C., Harris, N., Vance, D., 2001. Fluid-enhanced melting during prograde metamorphism. J. Geol. Soc. 158, 233–241.
Pullen, A., Kapp, P., DeCelles, P.G., Gehrels, G.E., Ding, L., 2011. Cenozoic anatexis and exhumation of Tethyan Sequence rocks in the Xiao Gurla Range, southwest Tibet. Tectonophysics 501, 28–40.
Quigley, M., Liangjun, Y., Xiaohan, L., Wilson, C.J.L., Sandiford, M., Phillips, D., 2006. $^{40}Ar/^{39}Ar$ thermochronology of the Kampa dome, southern Tibet: implications for tectonic evolution of the North Himalayan gneiss domes. Tectonophysics 421, 268–297.
Quigley, M.C., Liangjun, Y., Gregory, C., Corvino, A., Sandiford, M., Wilson, C.J.L., Xiaohan, L., 2008. U–Pb SHRIMP zircon geochronology and *T–t–d* history of the Kampa dome, southern Tibet. Tectonophysics 446, 97–113.
Rapp, R.P., Watson, E.B., 1986. Monazite solubility and dissolution kinetics – implications for the thorium and light rare-earth chemistry of felsic magmas. Contrib. Mineral. Petrol. 94, 304–316.
Ratschbacher, L., Frisch, W., Chen, C., Pan, G., 1992. Distributed deformation in southern and western Tibet during and after the India–Asia collision. J. Geophys. Res. 99, 19817–19945.
Replumaz, A., Karason, H., van der Hilst, R.D., Besse, J., Tapponnier, P., 2004. 4-D Evolution of SE Asia's mantle from geological reconstructions and seismic tomography. Earth Planet. Sci. Lett. 221, 103–115.
Richards, A., Argles, T., Harris, N., Parrish, R., Ahmad, T., Darbyshire, F., Draganits, E., 2005. Himalayan architecture constrained by isotopic tracers from clastic sediments. Earth Planet. Sci. Lett. 236, 773–796.
Sengupta, S., Acharyya, S.K., de Smith, J.B., 1996. Geochemical characteristics of the Abor volcanic rocks, NE Himalaya, India: nature and early Eocene magmatism. J. Geol. Soc. Lond. 153, 695–704.
Spear, F.S., 1995. Metamorphic Phase Equilibria and Pressure–Temperature–Time Paths. Mineralogical Society of America, Washington, DC, p. 799.
Stern, C.R., Kligfield, R., Schelling, D., Virdi, N.S., Futa, K., Peterman, Z.E., Amini, H., 1989. The bhagirathi leucogranite of the high Himalaya (Garhwal India); age, petrogenesis and tectonic implications. Geol. Soc. Am. Spec. Paper 232, 33–45.
Streckeisen, A., Le Maitre, R.W., 1979. A chemical approximation to the modal QAPF classification of the igneous rocks. Neues Jahrbuch Mineral 136, 169–206.
Suppe, J., Chou, G.T., Hook, S.C., McClay, K.R., 1992. Thrust Tectonics. Chapman and Hall.
Watson, E.B., Harrison, T.M., 1983. Zircon saturation revisited – temperature and composition effects in a variety of crustal magma types. Earth Planet. Sci. Lett. 64, 295–304.
Watson, E.B., Harrison, T.M., 2005. Zircon thermometer reveals minimum melting conditions on earliest Earth. Science 308, 841–844.
Watson, E.B., Wark, D.A., Thomas, J.B., 2006. Crystallization thermometers for zircon and rutile. Contrib. Mineral. Petrol. 151, 413–433.
Yin, A., 2006. Cenozoic evolution of the Himalayan Orogen as constrained by along-strike variations of structural geometry, exhumation history, and foreland sedimentation. Earth Sci. Rev. 76, 1–134.
Yin, A., Harrison, T.M., Ryerson, F.J., Chen, W., Kidd, W.S.F., Copeland, P., 1994. Tertiary structural evolution of the Gangdese thrust system, southeastern Tibet. J. Geophys. Res. 99, 18175–18201.
Yin, A., Dubey, C.S., Kelty, T.K., Webb, A.A.G., Harrison, T.M., Chou, C.Y., Célérier, J., 2009. Geologic correlation of the Himalayan orogen and Indian craton: Part 2.

Structural geology, geochronology, and tectonic evolution of the Eastern Himalaya. Geol. Soc. Am. Bull. 122, 360–395.
Yin, A., Harrison, T.M., 2000. Geologic evolution of the Himalayan–Tibetan orogen. Ann. Rev. Earth Planet. Sci. 28, 211–280.
Zeng, L., Gao, L.E., Xie, K., Zeng, J.L., 2011. Mid-Eocene high Sr/Y granites in the Northern Himalayan gneiss domes: melting thickened lower continental crust. Earth Planet. Sci. Lett. 303, 251–266.
Zhang, H.F., Harris, N., Parrish, R., Kelley, S., Zhang, L., Rogers, N., Argles, T., King, J., 2004a. Causes and consequences of protracted melting of the mid-crust exposed in the North Himalayan Antiform. Earth Planet. Sci. Lett. 228, 195–212.
Zhang, H.F., Harris, N., Parrish, R., Zhang, L., Zhao, Z., 2004b. U–Pb ages of Kude and Sajia leucogranites in Saffia Dome from North Himalaya and their geological implications. Chin. Sci. Bull. 49, 2087–2092.